Optical and Infrared Non-detection of the z=10 Galaxy behind Abell 1835

Smith, Graham; Sand, David J.; Egami, Eiichi; Stern, Daniel; Eisenhardt, Peter R.

DOI:
10.1086/497979

The Astrophysical Journal, 636:575–581, 2006 January 10

OPTICAL AND INFRARED NONDETECTION OF THE $z = 10$ GALAXY BEHIND ABELL 1835

Graham P. Smith,[1] David J. Sand,[1] Eiichi Egami,[2] Daniel Stern,[3] and Peter R. Eisenhardt[3]

Received 2005 March 11; accepted 2005 September 5

ABSTRACT

Gravitational lensing by massive galaxy clusters is a powerful tool for the discovery and study of high-redshift galaxies, including those at $z \geq 6$ likely responsible for cosmic reionization. Pelló et al. recently used this technique to discover a candidate gravitationally magnified galaxy at $z = 10$ behind the massive cluster lens Abell 1835 ($z = 0.25$). We present new Keck and *Spitzer Space Telescope* observations of the $z = 10$ candidate (hereafter #1916, following Pelló et al.'s nomenclature) together with a reanalysis of archival optical and near-infrared imaging from the *Hubble Space Telescope* and Very Large Telescope, respectively. Our analysis extends from the atmospheric cutoff at $\lambda_{\rm obs} \simeq 0.35$ μm out to $\lambda_{\rm obs} \simeq 5$ μm. The $z = 10$ galaxy is not detected in any of these data, including an independent reduction of Pelló et al.'s discovery *H*- and *K*-band imaging. We conclude that there is no statistically reliable evidence for the existence of #1916. We also assess the implications of our results for ground-based near-infrared searches for gravitationally magnified galaxies at $z \gtrsim 7$. The broad conclusion is that such experiments remain feasible, assuming that space-based optical and mid-infrared imaging are available to break the degeneracy with low-redshift interlopers (e.g., $z \sim 2-3$) when fitting spectral templates to the photometric data.

Subject headings: cosmology: observations — early universe — galaxies: evolution — galaxies: formation — infrared: galaxies

Online material: color figure

1. INTRODUCTION

Observations of distant quasi-stellar objects (QSOs; Becker et al. 2001; Fan et al. 2002) and the cosmic microwave background (Kogut et al. 2003) together suggest that the universe was reionized somewhere between $z \simeq 6$ and 20. Searching for the sources of reionizing photons is currently an intense observational effort. Most searches naturally concentrate on luminous systems, i.e., QSOs and luminous galaxies, at $z \sim 6-8$, as these should be easier to detect than less luminous and more distant objects. However, QSOs likely produced insufficient photons to accomplish reionization alone (Fan et al. 2001; Barger et al. 2003), and the same may be true of luminous ($L \gtrsim 0.3L^{\star}_{z=3.8}$) galaxies based on small samples from the *Hubble Space Telescope* Ultra Deep Field (*HST* UDF: Bouwens et al. 2004; Bunker et al. 2004; Yan & Windhorst 2004). This raises the important possibilities that reionization either occurred much earlier, or that the bulk of the reionizing photons were emitted by subluminous galaxies, i.e., $L \lesssim 0.1L^{\star}$.

The UDF studies operate close to the detection threshold of the deepest optical/near-infrared imaging available. It is therefore difficult to envisage substantial progress in the detection of more remote and/or less luminous galaxies via deep imaging of "blank fields" with the current generation of telescopes. With the advent of the *James Webb Space Telescope* still some years ahead, the magnifying power of massive galaxy cluster lenses is therefore a much-needed boost for the discovery power of *HST* and large ground-based telescopes. Indeed, the galaxy redshift record has been broken on several occasions with the help of the gravitational magnification of distant galaxies by foreground galaxy clusters (Mellier et al. 1991; Franx et al. 1997; Hu et al. 2002; Kneib et al. 2004a). The faint end of the luminosity function of Lyα emitters at $z = 5$ has also been constrained with the help of gravitational lensing (Santos et al. 2004; Ellis et al. 2001). Extension of these techniques to $z \gtrsim 7$ is therefore an important element of observational studies of cosmic reionization.

Pelló et al. (2004, hereafter P04) reported a gravitationally magnified ($\mu \sim 25-100$) galaxy at $z = 10$ (hereafter #1916, following P04's nomenclature) behind the foreground galaxy cluster A1835 ($z = 0.25$). This interpretation is based on nondetection in optical imaging from the ground (3 σ limits in a 0.″6 diameter aperture: $V \geq 27.4$, $R \geq 27.5$, and $I \geq 26.9$) and space (3 σ limit in a 0.″2 diameter aperture: $R_{702} \geq 27.2$), and the shape of the continuum at $\lambda_{\rm obs} \geq 1$ μm [using a 1.″5 aperture: $(J-H) \geq 0.6$, $(H-K) = -0.5 \pm 0.4$], which is reminiscent of the Lyman break selection technique (Steidel et al. 1996). P04 corroborated the putative Lyman break redshifted to $\lambda_{\rm obs} \simeq 1.3$ μm with an emission line at $\lambda_{\rm obs} = 1.3375$ μm with integrated flux of $(4.1 \pm 0.5) \times 10^{-18}$ ergs cm^{-2} s^{-1}, which they interpret as Lyα. Lower redshift interpretations of the line ([O II] at $z = 2.59$; [O III] at $z = 1.68$; Hα at $z = 1.04$) were discarded by P04 largely on the basis of the low probability of solutions at $z \lesssim 7$ when fitting synthetic spectral energy distributions (SEDs) to their photometric data. The most likely of these lower redshift solutions ($z = 2.59$) was further excluded on the basis of the dust extinction required to fit the photometric data ($A_V \geq 2$) and the absence of doublet structure in the observed emission line.

Based solely on the photometry [optical nondetection, red $(J-H)$, and blue $(H-K)$ colors] the $z = 10$ interpretation of #1916 is plausible. However, P04's preference for this solution over the lower redshift alternatives was controversial from the outset. For example, the emission line does not have the characteristic P Cygni profile of Lyα, and the different photometric apertures adopted in the optical (0.″6—smaller than the ground-based seeing disk) and near-infrared (1.″5—3 times the seeing disk) may suppress the likelihood of lower redshift solutions

[1] Department of Astronomy, California Institute of Technology, Mail Code 105-24, Pasadena, CA 91125; gps@astro.caltech.edu.
[2] Steward Observatory, University of Arizona, 933 North Cherry Avenue, Tucson, AZ 85721.
[3] Jet Propulsion Laboratory, California Institute of Technology, 4800 Oak Grove Drive, MS 169-327, Pasadena, CA 91109.

when fitting synthetic SEDs. Bremer et al. (2004) have also suggested that #1916 may either not exist or be intrinsically variable, based on their nondetection in the *H* band with the Near-Infrared Imager (NIRI) on Gemini-North, $H(3\ \sigma) > 26$, in contrast to P04's 4 σ detection of $H = 25.00 \pm 0.25$ with the Infrared Spectrometer And Array Camera (ISAAC) on the Very Large Telescope (VLT). The spectroscopic identification of #1916 is also in doubt. Weatherley et al. (2004) reanalyzed P04's spectroscopic data and failed to detect the emission line at $\lambda_{\rm obs} = 1.3375$ μm, citing spurious positive flux arising from variable hot pixels in the ISAAC array as the likely source of the discrepancy.

A1835 has been used previously as a gravitational telescope, for example, targeting submillimeter galaxies (SMGs; e.g., Smail et al. 2002) and galaxies with extremely red optical/near-infrared colors (Smith et al. 2002). One of the galaxies detected in these surveys, SMMJ 14011+0252, lies at $z = 2.56$ and suffers an estimated extinction of $1.8 \lesssim A_V \lesssim 6.5$ (Ivison et al. 2000). Bearing in mind recent discovery of galaxy groups at $z \sim 2-3$ associated with gravitationally lensed SMGs (Kneib et al. 2004b; Borys et al. 2004) and the strong clustering of SMGs (Blain et al. 2004), #1916 is plausibly at a similar redshift to SMMJ 14011+0252 and may also be obscured by dust. Further circumstantial evidence for a lower redshift interpretation of #1916 comes from Richard et al. (2003), who used the same spectroscopic data as presented by P04 to discover a strongly reddened star-forming galaxy at $z = 1.68$. This redshift coincides with the [O III] interpretation of P04's putative emission line at $\lambda_{\rm obs} = 1.3375$ μm.

In this paper, we address three questions: (1) is #1916 at $z \sim 2-3$, (2) is #1916 intrinsically variable, and (3) does #1916 exist? These tests exploit new optical and mid-infrared observations using the Keck I 10 m telescope and the *Spitzer Space Telescope*, respectively, plus an independent reduction of P04's *H*- and *K*-band imaging data from the VLT. Throughout this article we assume that the emission line at $\lambda_{\rm obs} = 1.3375$ μm is a false detection (Weatherley et al. 2004). In § 2 we present the new Keck and *Spitzer* data, explain in detail the rereduction of the archival VLT ISAAC data, and summarize the archival *Hubble Space Telescope* (*HST*) data. Then in § 3 we describe the analysis and key results, focusing on the three questions posed above; this section closes with a summary of the current observational status of #1916. Finally, we discuss the implications of our results for future ground-based near-infrared searches for galaxies at $z \gtrsim 7$ (§ 4) and summarize our conclusions (§ 5).

We assume $H_0 = 65$ km s^{-1} Mpc^{-1}, $\Omega_M = 0.3$, and $\Omega_\Lambda = 0.7$ throughout. Unless otherwise stated, all error bars are at 1 σ significance, photometric detection limits are at 3 σ significance, and upper and lower limits on colors are based on 3 σ detection thresholds in the nondetection filter. Magnitudes are stated in the AB system; conversion between the AB and Vega systems for the specific filters used in this paper are as follows: $\Delta_B = B_{\rm AB} - B_{\rm Vega} = -0.1$, $\Delta_V = 0.1$, $\Delta_R = 0.2$, $\Delta_{\rm F702W} = 0.3$, $\Delta_I = 0.5$, $\Delta_J = 0.9$, $\Delta_H = 1.4$, $\Delta_K = 1.9$, $\Delta_{3.6\,\mu{\rm m}} = 2.8$, and $\Delta_{4.5\,\mu{\rm m}} = 3.2$.

2. OBSERVATIONS AND DATA REDUCTION

We describe new and archival observations of #1916 in order of increasing wavelength, spanning the observed optical, near-infrared, and mid-infrared: spectroscopy with LRIS on Keck I ($0.35\ \mu{\rm m} \le \lambda_{\rm obs} \le 0.95\ \mu$m), imaging with WFPC2 on board *HST* ($\lambda_{\rm obs} = 0.7$ μm), near-infrared imaging with ISAAC on the European Southern Observatory's (ESO) VLT ($\lambda_{\rm obs} = 1.6$ and 2.2 μm), and Infrared Array Camera (IRAC) *Spitzer* observations at $\lambda_{\rm obs} = 3.6$ and 4.5 μm.

The detection of any optical flux from #1916 would eliminate the $z = 10$ interpretation (e.g., Stern et al. 2000). In contrast, optical nondetection would have several alternative interpretations, including the following: a galaxy at $z = 10$, as per P04; a dusty galaxy at $z \sim 2-3$; and the nonexistence of #1916. The mid-infrared observations (§ 2.4) should therefore help to constrain the amount of energy reradiated by dust in the $z \sim 2-3$ interpretation, and our rereduction of P04's VLT data also helps to clarify the possibility that #1916 may not exist, or may be variable (Bremer et al. 2004). The Keck and *Spitzer* data described in this section were collected and analyzed in parallel with those presented by Bremer et al. (2004).

2.1. *Keck Spectroscopy*

As part of a broad effort to secure spectroscopic redshifts of gravitational arcs spanning several observational programs (Smith et al. 2001, 2002, 2005; Sand et al. 2002, 2004, 2005; Edge et al. 2003; Sharon et al. 2005), we observed A1835 with LRIS (Oke et al. 1995) in multislit mode on the Keck I 10 m telescope[4] on UT 2004 March 29. A single mask was observed, including a slit targeting #1916. The purpose of this slit was to search for line emission in the $0.35\ \mu{\rm m} \le \lambda_{\rm obs} \le 0.95\ \mu$m wavelength range. For example, if #1916 does indeed lie at $z \simeq 2.6$ (§ 1), then Lyα may be detectable at $\lambda_{\rm obs} \simeq 0.44$ μm.

The observations totaled 3.6 ks, split into two exposures, using the D560 dichroic with the 400/8500 grating and the 400/3400 grism. On the red side the spectral dispersion was 1.86 Å pixel^{-1} with a pixel scale of 0.″214 pixel^{-1}, and on the blue side the spectral dispersion was 1.09 Å pixel^{-1} with a pixel scale of 0.″135 pixel^{-1}. Overhead conditions were moderate (FWHM $\simeq 1''$) and probably not photometric; however, a flux calibration was obtained using the spectrophotometric standard star HZ44 (Oke 1990). The data were debiased, flat-fielded, sky-subtracted, extracted, and calibrated in a standard manner within the IRAF.[5]

No flux at observed optical wavelengths has yet been detected at the position of #1916 (P04; Lehnert et al. 2005; § 2.2). We therefore did not expect to detect any continuum emission and concentrated instead on searching for faint emission lines of large equivalent width. Visual inspection of the reduced two-dimensional data revealed neither continuum nor line emission. To estimate the sensitivity limit, we extracted a one-dimensional trace from the center of the slit corresponding to the full width of the seeing disk and estimated the 3 σ detection limit per 5A spectral resolution element to be $\sim 4.5 \times 10^{-19}$ ergs s^{-1} cm^{-2} at $\lambda_{\rm obs} = 0.44$ μm, i.e., the observed wavelength at which Lyα would be found if #1916 is at $z = 2.6$.

2.2. *Archival Hubble Space Telescope Imaging*

A1835 has also been observed through the F702W filter with the WFPC2 camera on board *HST*.[6] We refer the reader to Smith et al. (2005) for details of these data and their reduction. P04 do not detect #1916 in these data (Table 1), although they neither explain how they reduced the data nor how the detection limit was calculated. Here, we use Smith et al.'s (2005) reduced

[4] The W. M. Keck Observatory is operated as a scientific partnership among the California Institute of Technology, the University of California, and NASA.

[5] IRAF is distributed by the National Optical Astronomy Observatory, which is operated by the Association of Universities for Research in Astronomy, Inc. (AURA), under cooperative agreement with the National Science Foundation.

[6] Based in part on observations with the NASA/ESA *Hubble Space Telescope* obtained at the Space Telescope Science Institute, which is operated by the Association of Universities for Research in Astronomy, Inc., under NASA contract NAS 5-26555.

TABLE 1
Summary of Photometry

Filter (1)	Telescope/Instrument (2)	FWHM (arcsec) (3)	Aperture Photometry[a] Pelló et al.[b] (arcsec) (4)	Aperture Photometry[a] This Paper (arcsec) (5)
V	CFHT/12k	0.76	$\geq$27.5 (0.6)	...
R	CFHT/12k	0.69	$\geq$27.6 (0.6)	...
R_{702}	*HST*/WFPC2	0.17	$\geq$27.2 (0.2)[c]	$\geq$27.0 (0.5)
I	CFHT/12k	0.78	$\geq$26.0 (0.6)	...
J	VLT/ISAAC	0.65	$\geq$25.6 (1.5)	...
H	VLT/ISAAC	0.50	25.00 $\pm$ 0.25 (1.5)	$\geq$25.0 (1.5)
K	VLT/ISAAC	0.38	25.51 $\pm$ 0.36 (1.5)	$\geq$25.0 (1.5)
3.6 μm	*Spitzer*/IRAC	1.7	...	$\geq$24.3 (5.1)
4.5 μm	*Spitzer*/IRAC	1.7	...	$\geq$24.3 (5.1)

[a] Each number in parentheses is the diameter of the aperture used for the respective photometric measurements. In § 4, P04's optical nondetections are rescaled to a photometric aperture of 2″ diameter (~3 times the seeing disk): $V \geq 26.2$, $R \geq 26.3$, and $I \geq 24.7$.

[b] We convert all of P04's optical detection limits and their 1 σ J-band detection to 3 σ limits.

[c] P04 do not state whether their R_{702} detection limit is in the Vega or AB system. We have assumed the former and converted it to AB in this table. P04 also do not explain how they reduced the WFPC2 data, specifically, whether the final pixel scale was different from the native 0.″0996 pixel^{-1} of the WFC detectors. In this table we have assumed that the 4 pixels over which this detection limit is measured (see P04 § 2.1) subtend a solid angle of 0.″0996 × 0.″0996. Given these uncertainties and the absence of this detection limit from P04's Table 1 and Fig. 3, we ignore P04's limit when attempting to reproduce their photometric redshift results in § 4.

frame, which has a pixel scale of 0.″0498 pixel^{-1} after drizzling. To simplify the analysis, we rebin the data back to the original pixel scale of 0.″0996 pixel^{-1} to minimize the impact of pixel-to-pixel correlations in the background noise when estimating the sensitivity limit of the data.

Visual inspection reveals no obvious flux at the position of #1916 in these data. To quantify this nondetection, we follow the same procedure as P04: we measured the background noise in apertures placed randomly into blank-sky regions of both frames near to the position of #1916. We ensure consistency with other wavelengths by matching the diameter of these apertures to a diameter 3 times that of the seeing disk, i.e., 0.″5. We obtain a 3 σ sensitivity limit in that aperture of $R_{702} = 27.0$ (Table 1).

2.3. *Archival VLT ISAAC Imaging*

Deep near-infrared imaging of A1835 was obtained by P04 with the ISAAC 1024 × 1024 Hawaii Rockwell array on ESO's 8 m VLT[7] in 2003 February. We reduced independently the H- and K-band data using standard IRAF tasks, paying careful attention to rejection of cosmetic defects in the ISAAC array, including bad pixels, and to conserve the noise properties of the data. We detail key features of the data reduction below.

1. Flat-fielding and sky subtraction were combined into a single step using a median of the eight frames temporally adjacent to each science frame. We refer to this step as "flat-fielding" and to the rolling temporal median frames as "sky-flats."

2. Flat-fielding was performed twice: first on the dark-subtracted frames, which were then registered and averaged to produce a first-pass reduced frame. This frame was then used to mask out flux from identified sources from the individual dark-subtracted frames, and these masked frames were then used to construct the sky-flats in a second-pass reduction. This approach minimizes the loss of flux from objects with angular extents comparable to the size of the dither pattern. This is important when searching for faint objects along lines of sight through the crowded cores of rich galaxy clusters, because the light from bright cluster galaxies effectively forms a spatially varying background against which the faint sources are detected. The goal of the second-pass flat field is to conserve this "background."

3. Independent bad pixel masks were made by sigma-clipping both the darks and the sky-flats. The former identifies 22,020 pixels (2.1% of the total array) as static, i.e., "bad," and the latter identifies the same 22,020 pixels plus an additional 12,373 pixels (a further 1.2% of the total array) as bad. The latter mask was adopted as the fiducial bad pixel mask.

4. Detector bias residuals were removed by subtracting the median along rows in individual flat-fielded frames after masking identified sources, in a manner similar to that described by Labbé et al. (2003).

5. The individual frames were integer pixel aligned. This has the important benefit of minimizing pixel-to-pixel correlations in the noise properties of each frame and thus the final stacked frame. Calculation of the background noise is therefore simplified relative to a reduction scheme based on subinteger pixel alignment of the individual frames.

6. No frames were rejected when making the final combination of the reduced, aligned frames. Two versions of the final stacked frame were made: a straight average and a weighted average; the weight of an individual frame was proportional to $(\sigma \times \mathrm{rms})^{-2}$, where σ is the FWHM of the seeing disk and rms is the root mean square per pixel of the noise in each frame. The weighted version of the final frame has slightly better image quality than the straight average. We therefore adopt it for the analysis described below.

The final reduced H- and K-band frames have seeing of FWHM = 0.″45 $\pm$ 0.″01 and 0.″34 $\pm$ 0.″02, respectively. Photometric calibration was achieved with the standard star observations that were interspersed with the science observations as part of P04's original program. We show extracts from the reduced H- and K-band frames in Figure 1. Visual inspection of both the fits frames and Figure 1 reveals no obvious flux

[7] Based in part on observations collected with the ESO VLT-UT1 Antu Telescope.

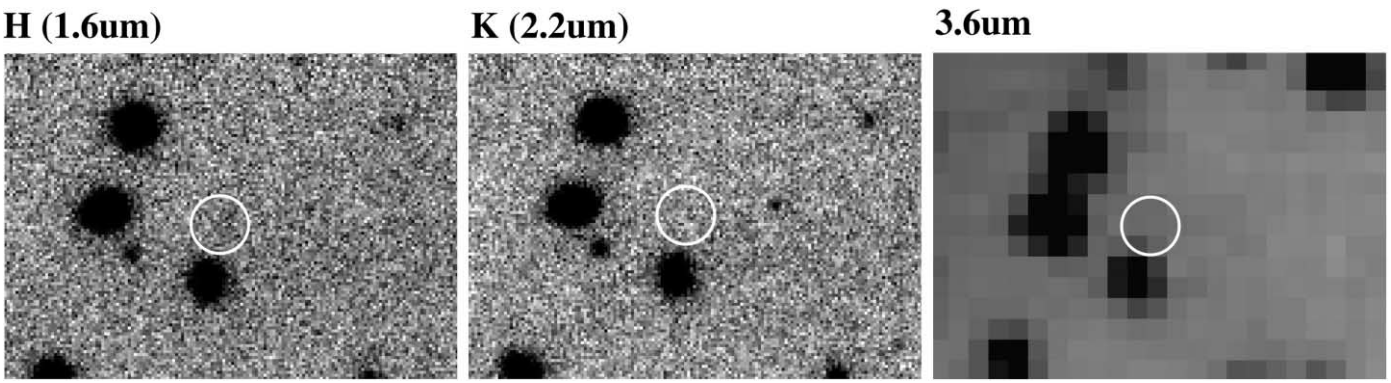

FIG. 1.—Infrared images of the $z = 10$ candidate at 1.6, 2.2, and 3.6 μm, respectively. The two left panels are based on our independent rereduction of P04's ISAAC data described in § 2.3. The white circles mark the position of #1916 from P04: there is no obvious sign of flux in any of these panels. Formal 3 σ detection limits are $H \geq 25$, $K \geq 25$, and $F \leq 0.75$ μJy. North is up, and east is to the left. Each panel is $23'' \times 16''$.

at the location of #1916 in either the H or K band. Following P04 we again randomly insert 1.″5 diameter apertures (roughly 3 times the seeing disk) into blank-sky regions near to the position of #1916, obtaining 3 σ sensitivity limits in this aperture of $H = 25.0$ and $K = 25.0$.

2.4. *Spitzer IRAC Imaging*

A1835 was observed with IRAC (Fazio et al. 2004) on board *Spitzer*[8] on UT 2004 January 16 in the 3.6, 4.5, 5.8, and 8.0 μm channels. Here we discuss the two shortest wavelength, more sensitive, observations. Twelve and eighteen 200 s exposures were accumulated at 3.6 and 4.5 μm, respectively, using the small-step cycling dither pattern. The Basic Calibrated Data (BCD) were combined using custom routines to produce the final stacked frame with a pixel scale of 0.″6 pixel^{-1}. We rebinned the data back to the original pixel scale of 1.″2 pixel^{-1} to eliminate correlations in the background noise.

Visual inspection of the final frames again indicates that there is no flux at the position of #1916 (Fig. 1). To quantify this nondetection, we follow the same procedure as P04, as described in § 2.2. We used 5.″1 diameter apertures, i.e., 3 times the seeing disk of the IRAC observations to obtain 3 σ sensitivity limits of $F(3.6\ \mu\text{m}) = 0.75$ μJy and $F(4.5\ \mu\text{m}) = 0.75$ μJy, respectively.

3. ANALYSIS AND RESULTS

The objective of this section is to answer the three questions posed in § 1: (1) is #1916 at $z \sim 2$–3, (2) is #1916 intrinsically variable, and (3) does #1916 exist? Preliminary inspection of the data in § 2 indicates that no flux is detected at the position of #1916 at any wavelength to date. Combining this with Bremer et al.'s (2004) more sensitive nondetection of $H(3\ \sigma) > 26.0$, it is tempting to leap to the third question and reply "no". We adopt a more conservative approach.

3.1. *Is* #1916 *at* $z \sim 2$–3*?*

This test concentrates on the optical data because the detection of any flux shortward of the putative Lyman limit of a galaxy at $z \simeq 10$ would immediately discount that interpretation. The red observed optical/near-infrared SED described by P04 could then be naturally explained by a dusty galaxy at $z \sim 2$–3, perhaps associated with the SMGs that lie within $\sim 30''$ ($\sim$200–300 kpc in projection at $z \sim 2$–3) of #1916 (Ivison et al. 2000; Smail et al. 2005).

Our new nondetection of #1916 with LRIS (§ 2.1), coupled with confirmation of P04's nondetection with *HST* WFPC2 and Lehnert et al.'s (2005) nondetection in the V band with VLT FORS, are mutually consistent in the sense that no optical flux has been detected at this position to date. However, these nondetections are consistent with all of the following: $z = 10$, extreme dust obscuration at $z \sim 2$–3, an intrinsically variable source, and nonexistence. The result of this test is therefore inconclusive.

3.2. *Is* #1916 *Intrinsically Variable?*

The objective of this section is to test Bremer et al.'s (2004) proposal that #1916 is intrinsically variable. If P04's photometry ($H = 25.00 \pm 0.25$ and $K = 25.51 \pm 0.51$) is reproducible using our independent reduction of their near-infrared data, then the variable hypothesis would be supported. If not, then the idea that #1916 does not exist would gain credibility (§ 3.3).

We attempt to reproduce P04's analysis using SExtractor (Bertin & Arnouts 1996). SExtractor was configured to locate all sources with at least 7 pixels that are ≥ 0.75 σ pixel^{-1} above the background—i.e., a signal-to-noise ratio of $\gtrsim 2$ per resolution element, based on the H-band seeing disk of FWHM = 0.″45 $\pm$ 0.″01 (§ 2.3) and the 0.″15 pixel^{-1} scale of the ISAAC pixels. We also smoothed the data with a Gaussian filter that matched the FWHM of the observed point sources, i.e., a Gaussian of FWHM = 3 pixels. In this configuration SExtractor failed to detect a source at the position of #1916. We therefore experimented with different smoothing schemes, both increasing and decreasing the full width of the Gaussian filter. A "detection" was only possible with the smallest available filter—FWHM = 1.5 pixels, i.e., half the width of the seeing disk—yielding $H = 25.3 \pm 0.6$. Experimentation with block filters produced similar results, in that a detection was not possible with any of the standard SExtractor block filters: 3×3, 5×5, and 7×7 pixels. We also analyzed the K-band data in exactly the same manner and failed to detect anything at the position of #1916 with any Gaussian or block filter.

The H-band segmentation map produced when smoothing with the FWHM = 1.5 pixel Gaussian reveals that the detection is very elongated, with a width of 1–2 pixels and a length of $\sim$5 pixels. The orientation of these pixels is consistent with the orientation of #1916 reported by P04. It is important to stress

[8] This work is based in part on observations made with the *Spitzer Space Telescope*, which is operated by the Jet Propulsion Laboratory, California Institute of Technology, under a contract with NASA.

that the motivation for filtering data with a kernel that matches the resolution element of the data is to suppress false detections. The collection of pixels identified by SExtractor at the position of #1916 was only "detectable" with a smoothing kernel that has a linear scale half that of the resolution element of the data. It is therefore instructive to consider how many such $\sim 2\ \sigma$ blobs exist within the ISAAC data. In a single $1\farcs5$ diameter aperture (i.e., matching that used for the photometry described above) placed randomly in these H-band data, there is a 5% chance of detecting a $2\ \sigma$ noise fluctuation—i.e., a spurious detection. However, the ISAAC array (1024×1024 pixels, each pixel $0\farcs15 \times 0\farcs15$) contains of order 10^4 independent photometric apertures of $1\farcs5$ diameter. The H-band frame therefore contains ~ 500 noise fluctuations of $2\ \sigma$ significance.

The only reasonable conclusion to draw from this analysis is that #1916 is not detected in our independent reduction of P04's data. We therefore place $3\ \sigma$ limits on the flux at this position of $H \geq 25.0$ and $K \geq 25.0$ (§ 2.3). The only wavelength at which two directly comparable observations are available is in the H band. Combining our nondetection with that of Bremer et al. (2004), we conclude that there is no evidence for variability of #1916, and that (if it exists) its H-band flux is fainter than $H = 26$ at $3\ \sigma$ significance (Bremer et al. 2004).

3.3. *Does* #1916 *Exist?*

The results of the preceding two sections were derived from nondetection of #1916 across the broadest wavelength range to date: $0.35\ \mu\text{m} \leq \lambda_{\text{obs}} \leq 5\ \mu\text{m}$. We now combine all of these nondetections to address the question of whether #1916 exists. The data force us to conclude that there is no statistically sound evidence that #1916 exists. The balance of probability is that #1916 was a false detection in P04's discovery observations. New observational data yielding statistically sound detections are required before P04's claim that #1916 is the most distant galaxy yet discovered can be resurrected. We consider this unlikely, but we hope to be surprised by Pelló et al.'s forthcoming *HST* observations.

4. DISCUSSION

4.1. *The Near-Infrared Nondetection*

We first discuss possible reasons for the difference between our nondetection of #1916 and P04's ~ 3–$4\ \sigma$ near-infrared detections. We single out two data reduction steps (§ 2.3) for discussion: the efficiency of bad pixel rejection and the conservation of noise properties.

4.1.1. *Efficiency of Bad Pixel Rejection*

The efficiency with which bad pixels are identified can affect estimates of the signal coming from faint sources—if some bad pixels are not identified, they could enhance the flux detected by SExtractor. In § 2.3 we used two different methods to identify bad pixels, finding a small but potentially important difference between the two methods. To assess the impact of reduced efficiency of bad pixel identification, we made a mask image that contained the 12,373 bad pixels identified only in the bad pixel mask generated from the sky-flats. We then made one copy of the mask per science frame and integer pixel shifted them to match the observed dither pattern. Finally, we took the weighted average of these aligned mask frames and summed the pixel counts in a $1\farcs5$ diameter aperture centered on #1916. From this we concluded that seven bad pixels that are only identified in our sky-flat bad pixel maps fall within the final photometric aperture. We estimate that if not identified and excluded from the analysis, these pixels could increase the flux estimates by several tenths of a magnitude.

4.1.2. *Conservation of Noise Properties*

The approach to resampling (or not) the individual frames during the data reduction process, especially the alignment of individual frames, affects the noise properties of the final stacked frame. If the individual frames are resampled, for example, by subinteger pixel aligning them immediately prior to producing the final stacked frame, then the noise in the stacked frame is correlated. Such pixel-to-pixel correlations are generally absent from integer pixel aligned data, thus simplifying the noise properties of the final frame. Neither subinteger nor integer pixel alignment is intrinsically correct. The relevant issue is correct measurement of the noise in each case—this is critical to assess accurately the statistical significance of sources detected close to the sensitivity limit of the data. Specifically, if the pixel-to-pixel correlations in subinteger pixel aligned data are not included in the error analysis, then the noise is underestimated and the statistical significance of the detection is overestimated (Casertano et al. 2000). We integer pixel aligned the individual frames in § 2.3 in order to simplify the error analysis. We now estimate by how much we would have underestimated the noise if we had subinteger pixel aligned the individual frames and then ignored the pixel-to-pixel correlations when calculating noise level. This is achieved by simply subinteger aligning the individual frames and recombining them using a weighted average. Ignoring any resulting pixel-to-pixel correlations, we obtain a $3\ \sigma$ threshold of $H = 25.2$, which is slightly fainter than our threshold of $H = 25.0$.

In summary, it is plausible that the difference between our near-infrared nondetection and P04's detection of #1916 using the same raw data can at least in part be explained by the efficiency of bad pixel identification and treatment of correlated noise.

4.2. *Implications for Future Work*

We now discuss the implications of our results for future work, focusing on the feasibility of searches for gravitationally magnified stellar systems at $z \gtrsim 7$ using ground-based near-infrared data. We begin by noting that, had their photometry been reliable, P04's original $z = 10$ interpretation of #1916 would have been plausible, based solely on the photometric data. We therefore adopt P04's optical and near-infrared photometry as being representative of what may be expected from similar future experiments—i.e., optical nondetections in several filters based on a few hours of observations with a 4 m class telescope, a nondetection in a single red optical filter with *HST*, ~ 3–$4\ \sigma$ detections in two near-infrared filters, and possibly observations with *Spitzer* IRAC. Specifically, we investigate the degeneracy between $z \gtrsim 7$ interpretations of such data with lower redshift alternatives and how such degeneracies might be broken.

We use version 1.1 of Hyperz[9] (Bolzonella et al. 2000) to fit standard Bruzual & Charlot (1993) single stellar population models (Burst, E, Sa, Sc, and Im) to the photometric data. We assume a Calzetti et al. (2000) extinction law, allow dust extinction in #1916 to lie in the range $0 \leq A_V \leq 4$, adopt $E(B-V) = 0.03$ for extinction within the Milky Way (Schlegel et al. 1998), and use Madau's (1995) prescription for absorption by the intergalactic medium. In each case described below, if we fit the models to all available photometric information across the full redshift range ($0 \leq z \leq 11$), then we obtain $\chi^2 \lesssim 1$ (all χ^2 values

[9] See http://webast.ast.obs-mip.fr/hyperz.

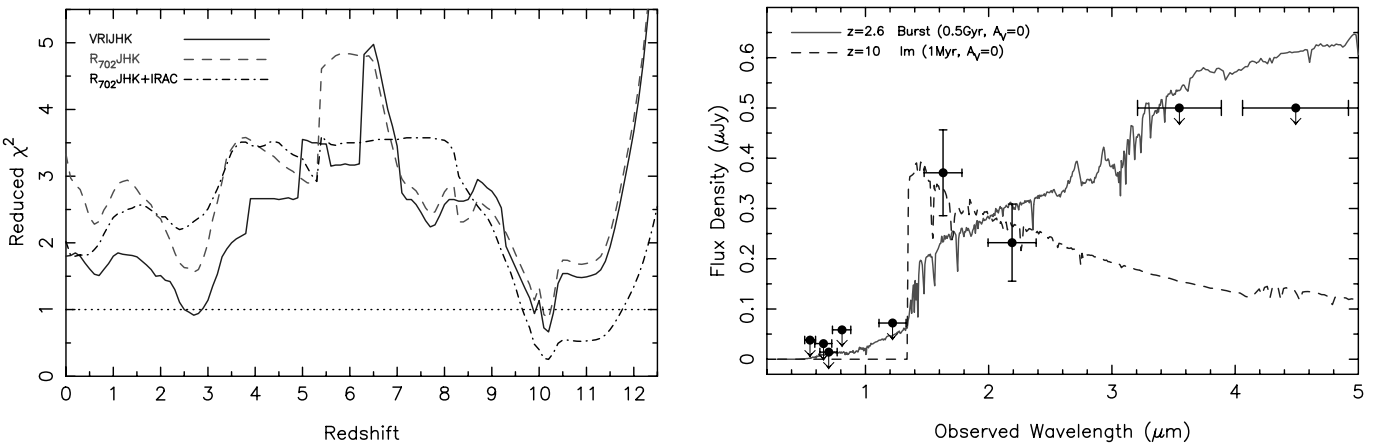

FIG. 2.—*Left*: Reduced χ^2 as a function of photometric redshift and the filters used in the model fits. The dashed curve has been offset +0.2 in the *Y*-direction for clarity. This panel demonstrates that P04's discovery photometry (*VRIJHK*) is degenerate between $z \simeq 2.6$ and $z = 10$ (*solid curve*). Adding in sensitive space-based detection thresholds from *HST* and *Spitzer* IRAC (*dashed and dot-dashed curves*, respectively) lifts this degeneracy. *Right*: The best-fit spectral templates to the $R_{702}JHK$-band photometry at $z = 2.6$ (*solid line*) and $z = 10$ (*dashed line*). The IRAC detection thresholds are also marked to illustrate the power of these data to discriminate between low- and high-redshift interpretations of the shorter wavelength data. [*See the electronic edition of the Journal for a color version of this figure.*]

are quoted per degree of freedom) for all redshifts beyond $z \simeq 7$. This is because the models are defined to have zero flux shortward of the Lyman limit ($\lambda_{\rm rest} = 0.0912$ μm). At $z \gtrsim 6$, the models also have negligible flux shortward of Lyα ($\lambda_{\rm rest} = 0.1215$ μm) due to the Lyman forests and Gunn-Peterson absorption. These two spectral features are progressively redshifted longward of the observed optical filters at high redshift, rendering the shorter wavelength detection limits irrelevant to the fits. The goodness of fit is therefore systematically overestimated at high redshift if all photometric information is included in the fit across the full redshift range. We therefore fit the models to the data in a series of redshift chunks—only the photometric information that lies longward of redshifted Lyα is considered in each redshift chunk. The results described below are insensitive to whether or not the Lyman limit is substituted for Lyα.

First, we fit the models to P04's *VRIJHK*-band ground-based photometry (i.e., the *VRIJ*-band detection limits and the *HK*-band detections listed in col. [4] of Table 1). Note that P04 used different sized apertures for the near-infrared (1.″5) and optical (0.″6) photometry, respectively. We find two acceptable solutions, $z \simeq 2.6$ and $z \simeq 10$ (Fig. 2), neither of which require any dust obscuration within #1916, the latter having the lower formal χ^2 value. We also scale P04's ground-based optical nondetections to that appropriate for a consistent photometric aperture of 3 times the seeing disk at all wavelengths ($V \geq 26.2$, $R \geq 26.3$, and $I \geq 24.7$). This marginally improves the goodness of fit of the $z \simeq 2.6$ solution and is otherwise indistinguishable from the original fit. We retain the matched photometric apertures for the remainder of this analysis.

To improve the discrimination between low- and high-redshift solutions, we add the sensitive *HST* WFPC2 detection threshold of $R_{702} \geq 27.0$ (Table 1) to the photometric constraints. We fit the synthetic SEDs to the combined $VRR_{702}IJHK$ data set. The goodness of fit of the $z \simeq 2.59$ solution is marginally worse relative to the *VRIJHK*-band analysis, because the most stringent optical nondetection comes from the R_{702} band. However, in general, the χ^2 as a function of redshift is indistinguishable between this fit and the *VRIJHK*-band fits. This is probably because the χ^2 is dominated by the nondetections in six out of the eight observed filters. To test this we refit the models, limiting the data to just the $R_{702}JHK$ bands, i.e., the most sensitive nondetection (R_{702}), the reddest nondetection (J), and the two detections (HK). The impact of the sensitive detection limit from the *HST* data is now clearly evident in the new χ^2 distribution, as shown in Figure 2. The only acceptable fit to the $R_{702}JHK$-band data is at $z \simeq 10$.

We show the best-fit SEDs at $z = 2.6$ and 10, based on the $R_{702}JHK$-band data in the right panel of Figure 2. This demonstrates the potential power of IRAC photometry to further discriminate between low- and high-redshift interpretations of candidate high-redshift galaxies. The SED of low-redshift solutions (e.g., $z \simeq 2.6$) is red at $\lambda_{\rm obs} \sim 3-5$ μm, and the SED of high-redshift solutions ($z \simeq 10$) is blue at similar wavelengths. We add the detection limits obtained at $\lambda_{\rm obs} = 3.6$ and 4.5 μm to the $R_{702}JHK$-band data and refit the spectral templates. The result is shown in the left panel of Figure 2: the reduced χ^2 of the $z \simeq 2.6$ solution is now in excess of 2, and the only redshifts that achieve an acceptable fit to the data are $9.5 \lesssim z \lesssim 11.5$.

In summary, a single sensitive nondetection derived from *HST* imaging, combined with deep ground-based near-infrared imaging and ~2400 s integrations with *Spitzer* IRAC at 3.6 and 4.5 μm can break the degeneracy between low- and high-redshift interpretations of candidate $z \gtrsim 7$ stellar systems (see also Egami et al. 2005; Eyles et al. 2006). While this is not an exhaustive study, it demonstrates that despite the demise of #1916, searches for gravitationally magnified galaxies at extremely high redshifts using ground-based near-infrared data remain feasible when combined with sensitive space-based optical and mid-infrared data.

5. CONCLUSIONS

We have analyzed new and archival observations of the $z = 10$ galaxy #1916 behind the foreground galaxy cluster lens A1835 ($z = 0.25$) spanning 0.35 μm $\leq \lambda_{\rm obs} \leq 5$ μm. Statistically significant flux is not detected in any of these data, including our independent reanalysis of P04's *H*- and *K*-band discovery data. The 3 σ detection thresholds are as follows: $F(\lambda_{\rm obs} = 0.44\ \mu{\rm m}) \gtrsim 4.5 \times 10^{-19}$ ergs s^{-1} cm^{-2} per spectral resolution element, $R_{702} \geq 27.0$, $H \geq 25.0$, $K \geq 25.0$, $F(3.6\ \mu{\rm m}) \leq 0.75$ μJy, and $F(4.5\ \mu{\rm m}) \leq 0.75$ μJy, where the photometric limits are calculated in apertures with a diameter 3 times that of the seeing disk.

Combining these results with those of Bremer et al. (2004) and Weatherley et al. (2004), we are therefore forced by the data to conclude that there is no statistically sound evidence for the existence of #1916. We also show that inefficient bad pixel

rejection and issues relating to the calculation of the background noise can broadly account for the differences between P04's near-infrared photometry and our own using the same data. The balance of probability is therefore that #1916 was a false detection in P04's analysis. From a broader perspective, the demise of #1916 warns of the hazards of operating close to the detection threshold of deep ground-based near-infrared data.

The need for gravitational magnification to boost the observed flux of faint ($L \lesssim 0.1L^{\star}$) galaxies at $z \sim 6-8$ and populations of galaxies at still higher redshifts (see § 1) is undiminished by our results on #1916. However, an important issue is whether it is feasible to find such galaxies using ground-based facilities. We explore this issue using Hyperz to fit synthetic spectral templates to representative data. Our main conclusions are that deep near-infrared imaging similar to that presented by P04 in combination with a single sensitive optical nondetection from *HST* imaging and moderate-depth *Spitzer* IRAC imaging at 3.6 and 4.5 μm can discriminate between low- (e.g., $z \sim 2-3$) and high- (e.g., $z \gtrsim 7$) redshift solutions with strong statistical significance. In summary, ground-based near-infrared surveys of massive galaxy cluster lenses with 10 m class telescopes remain a powerful tool for the discovery of intrinsically faint galaxies ($L \lesssim 0.1L^{\star}$) at $z > 7$ that may be responsible for cosmic reionization. Future surveys should combine these data with sensitive space-based optical and mid-infrared observations.

We acknowledge the bold efforts of Roser Pelló and collaborators, and G. P. S. acknowledges cordial discussions with Roser in Lausanne during the summer of 2004. Special thanks go to Jean-Paul Kneib for making the raw near-infrared imaging data available. G. P. S. acknowledges the Caltech Optical Observatories Time Allocation Committee (TAC) for enthusiastic support, and thanks Richard Ellis and Avishay Gal-Yam for helpful comments on drafts of the manuscript. Thanks also go to Malcolm Bremer, Michael Cooper, Joe Jensen, Dan Stark, Chuck Steidel, and Dave Thompson for a variety of discussions and assistance. D. J. S. thanks Dawn Erb, Alice Shapley, Naveen Reddy, and Tommaso Treu for assistance with the LRIS data reduction, and acknowledges financial support from NASA's Graduate Student Research Program, under NASA grant NAGT-50449. D. S. and P. R. M. E. acknowledge support from NASA. We recognize and acknowledge the cultural role and reverence that the summit of Mauna Kea has within the Hawaiian community. We are fortunate to conduct observations from this mountain.

REFERENCES

Barger, A. J., et al. 2003, AJ, 126, 632
Becker, R. H., et al. 2001, AJ, 122, 2850
Bertin, E., & Arnouts, S. 1996, A&AS, 117, 393
Blain, A. W., Chapman, S. C., Smail, I., & Ivison, R. 2004, ApJ, 611, 725
Bolzonella, M., Miralles, J.-M., & Pelló, R. 2000, A&A, 363, 476
Borys, C., et al. 2004, MNRAS, 352, 759
Bouwens, R. J., et al. 2004, ApJ, 616, L79
Bremer, M. N., Jensen, J. B., Lehnert, M. D., Förster-Schreiber, N. M., & Douglas, L. 2004, ApJ, 615, L1
Bruzual, A. G., & Charlot, S. 1993, ApJ, 405, 538
Bunker, A. J., Stanway, E. R., Ellis, R. S., & McMahon, R. G. 2004, MNRAS, 355, 374
Calzetti, D., Armus, L., Bolin, R. C., Kinney, A. L., Koornneef, J., & Storchi-Bergmann, T. 2000, ApJ, 533, 682
Casertano, S., et al. 2000, AJ, 120, 2747
Edge, A. C., Smith, G. P., Sand, D. J., Treu, T., Ebeling, H., Allen, S. W., & van Dokkum, P. G. 2003, ApJ, 599, L69
Egami, E., et al. 2005, ApJ, 618, L5
Ellis, R. S., Santos, M. R., Kneib, J.-P., & Kuijken, K. 2001, ApJ, 560, L119
Eyles, L., Bunker, A., Stanway, E., Lacy, M., Ellis, R. S., & Doherty, M. 2006, MNRAS, in press (astro-ph/0502385)
Fan, X., Narayanan, V. K., Strauss, M. A., White, R. L., Becker, R. H., Pentericci, L., & Rix, H.-W. 2002, AJ, 123, 1247
Fan, X., et al. 2001, AJ, 122, 2833
Fazio, G. G., et al. 2004, ApJS, 154, 10
Franx, M., Illingworth, G. D., Kelson, D. D., van Dokkum, P. G., & Tran, K.-V. 1997, ApJ, 486, L75
Hu, E. M., Cowie, L. L., McMahon, R. G., Capak, P., Iwamuro, F., Kneib, J.-P., Maihara, T., & Motohara, K. 2002, ApJ, 568, L75
Ivison, R. J., Smail, I., Barger, A. J., Kneib, J.-P., Blain, A. W., Owen, F. N., Kerr, T. H., & Cowie, L. L. 2000, MNRAS, 315, 209
Kneib, J.-P., Ellis, R. S., Santos, M. R., & Richard, J. 2004a, ApJ, 607, 697
Kneib, J.-P., van der Werf, P. P., Kraiberg Knudsen, K., Smail, I., Blain, A. W., Frayer, D., Barnard, V., & Ivison, R. 2004b, MNRAS, 349, 1211
Kogut, A., et al. 2003, ApJS, 148, 161
Labbé, I., et al. 2003, AJ, 125, 1107
Lehnert, M. D., Förster Schreiber, N. M., & Bremer, M. E. 2005, ApJ, 624, 80
Madau, P. 1995, ApJ, 441, 18
Mellier, Y., Fort, B., Soucail, G., Mathez, G., & Cailloux, M. 1991, ApJ, 380, 334
Oke, J. B. 1990, AJ, 99, 1621
Oke, J. B., Cohen, J. G., Carr, M., Cromer, J., Dingizian, A., & Harris, F. H. 1995, PASP, 107, 375
Pelló, R., Schaerer, D., Richard, J., Le Borgne, J.-F., & Kneib, J.-P. 2004, A&A, 416, L35 (P04)
Richard, J., Schaerer, D., Pelló, R., Le Borgne, J.-F., & Kneib, J.-P. 2003, A&A, 412, L57
Sand, D. J., Treu, T., & Ellis, R. S. 2002, ApJ, 574, L129
Sand, D. J., Treu, T., Ellis, R. S., & Smith, G. P. 2005, ApJ, 627, 32
Sand, D. J., Treu, T., Smith, G. P., & Ellis, R. S. 2004, ApJ, 604, 88
Santos, M. R., Ellis, R. S., Kneib, J.-P., Richard, J., & Kuijken, K. 2004, ApJ, 606, 683
Schlegel, D. J., Finkbeiner, D. P., & Davis, M. 1998, ApJ, 500, 525
Sharon, K., et al. 2005, ApJ, 629, L73
Smail, I., Ivison, R. J., Blain, A. W., & Kneib, J.-P. 2002, MNRAS, 331, 495
Smail, I., Smith, G. P., & Ivison, R. J. 2005, ApJ, 631, 121
Smith, G. P., Kneib, J.-P., Ebeling, H., Csozke, O., & Smail, I. 2001, ApJ, 552, 493
Smith, G. P., Kneib, J.-P., Smail, I., Mazzotta, P., Ebeling, H., & Czoske, O. 2005, MNRAS, 359, 417
Smith, G. P., Smail, I., Kneib, J.-P., Davis, C. J., Takamiya, M., Ebeling, H., & Czoske, O. 2002, MNRAS, 333, L16
Steidel, C. C., Giavalisco, M., Pettini, M., Dickinson, M. E., & Adelberger, K. L. 1996, ApJ, 462, L17
Stern, D., Eisenhardt, P., Spinrad, H., Dawson, S., van Breugel, W., Dey, A., de Vries, W., & Stanford, S. A. 2000, Nature, 408, 560
Weatherley, S. J., Warren, S. J., & Babbedge, T. S. R. 2004, A&A, 428, L29
Yan, H., & Windhorst, R. 2004, ApJ, 600, L1